Supplementary Information (SI) for Materials Advances.

Optimized Grain Growth in $CsPbBr_3$ Thick Films Using Mist-Assisted Dissolution-Recrystallization for Enhanced Optoelectronic Performance

Monet R. Brown; Susana Borbon-Rojas; Leunam Fernandez-Izquierdo; Ross Haroldson; Manuel Quevedo-Lopez.*

Department of Materials Science and Engineering, The University of Texas at Dallas, 2601 North Floyd Road RL10, Richardson, Texas 75080, United States.

SUPPLEMENTAL INFORMATION

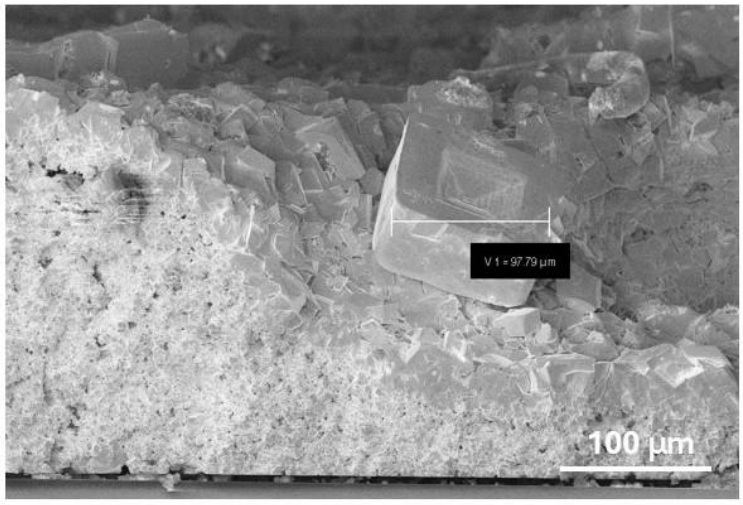

Figure S1: SEM of film recrystallized with pure DMSO

The grain size distribution in film treated with pure DMSO was calculated to be 9.53 ± 8.51, which is the largest variation in grain size across all variables. This is consistent with the significant grain size distribution observed in the SEM image (**Figure S1**).

Table S1: Tabulation of crystalline composition, average grain size, and crystallite size as a glo

Recrystallization Conditions		**Phase(s)**	**Avg. Grain Size (µm)**	**Crystallite Size (nm)**
Temperature	**Mist Con.**			
As Deposited	**-**	$CsPbBr_3$ (Ortho.)	0.83 ± 0.28	40.92 ± 2.66
60 ˚C	**0.1 M**	$CsPbBr_3$ (Ortho.)	2.09 ± 0.8	44.43 ± 1.63
	0.2 M	$CsPbBr_3$ (Ortho.) + $CsPb_2Br_5$ (Tetr.) + Cs_4PbBr_6 (Rh)	1.1 ± 0.4	64.55 ± 13.07
	0.4 M	$CsPbBr_3$ (Ortho.) + $CsPb_2Br_5$ (Tetr.) + Cs_4PbBr_6 (Rh)	0.978 ± 0.3	89.62 ± 17.82
85 ˚C	**0.1 M**	$CsPbBr_3$ (Ortho.)	3.19 ± 1.57	44.22 ± 10.08
	0.2 M	$CsPbBr_3$ (Ortho.)	1.85 ± 0.78	63.71 ± 17.74
	0.4 M	$CsPbBr_3$ (Ortho.) + Cs_4PbBr_6 (Rh)	1.45 ± 0.61	54.88 ± 4.735
110 ˚C	**0.1 M**	$CsPbBr_3$ (Ortho.)	1.91 ± 0.67	35.76 ± 0.48
	0.2 M	$CsPbBr_3$ (Ortho.)	1.78 ± 0.48	61.61 ± 23.25
	0.4 M	$CsPbBr_3$ (Ortho.)	1.52 ± 0.73	125.48 ± 9.56

Section S1: Crystallite size was calculated using the Scherrer equation as follows:

$$\tau = \frac{K\lambda}{\beta cos\theta}$$

Where τ is the mean size of the ordered crystalline domains, K is a dimensionless shape factor, λ is the X-ray wavelength, β is the line broadening at the full width half maximum of the XRD peak, and θ is the Bragg angle.[26]

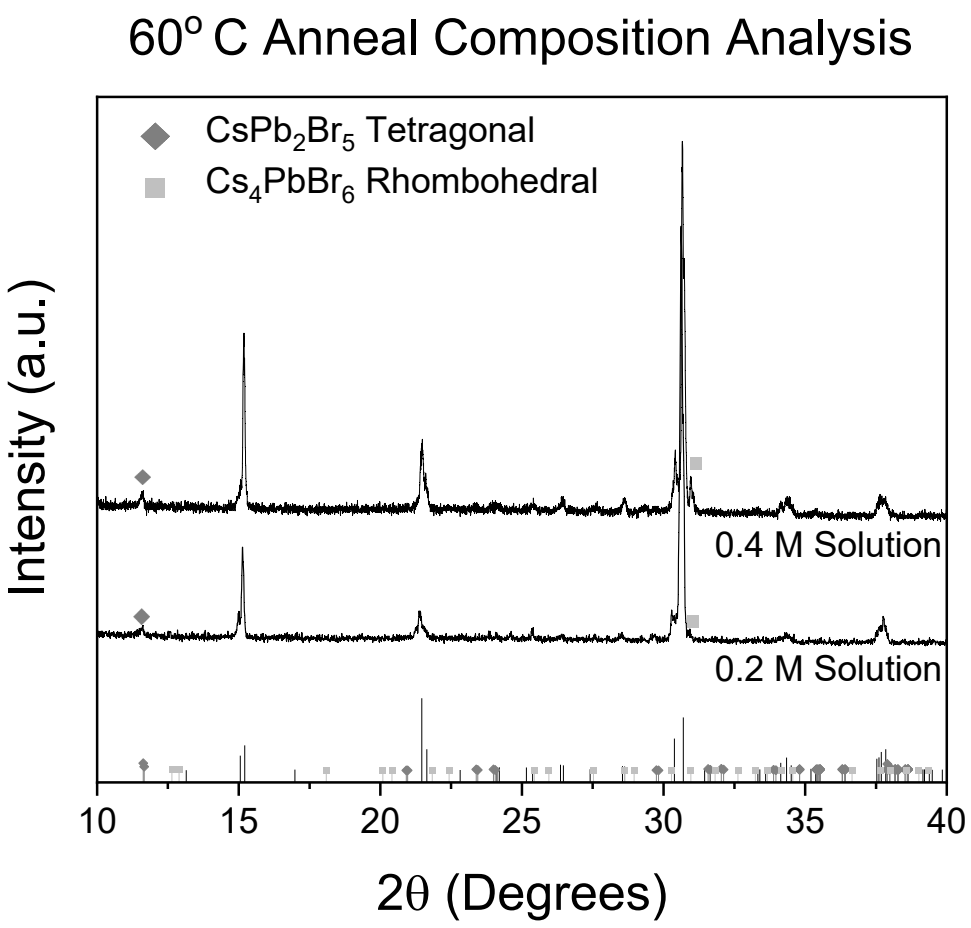

Figure S2: Compositional analysis of films annealed at 60 °C compared to Orthorhombic $CsPbBr_3$ PDF # 01-072-7929, Tetragonal $CsPb_2Br_5$ PDF # 00-054-0753 and Rhombohedral Cs_4PbBr_6 PDF # 01-077-8224.

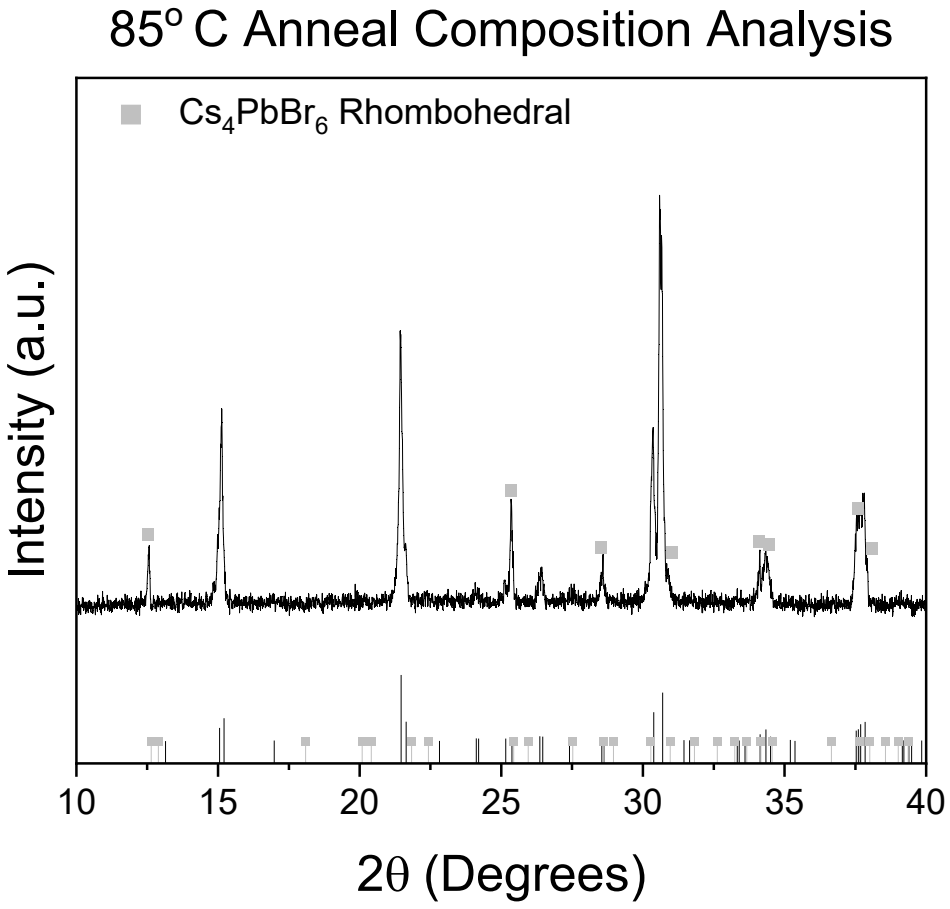

Figure S3: Compositional analysis of films annealed at 85 °C compared to Orthorhombic $CsPbBr_3$ PDF # 01-072-7929 and Rhombohedral Cs_4PbBr_6 PDF # 01-077-8224.

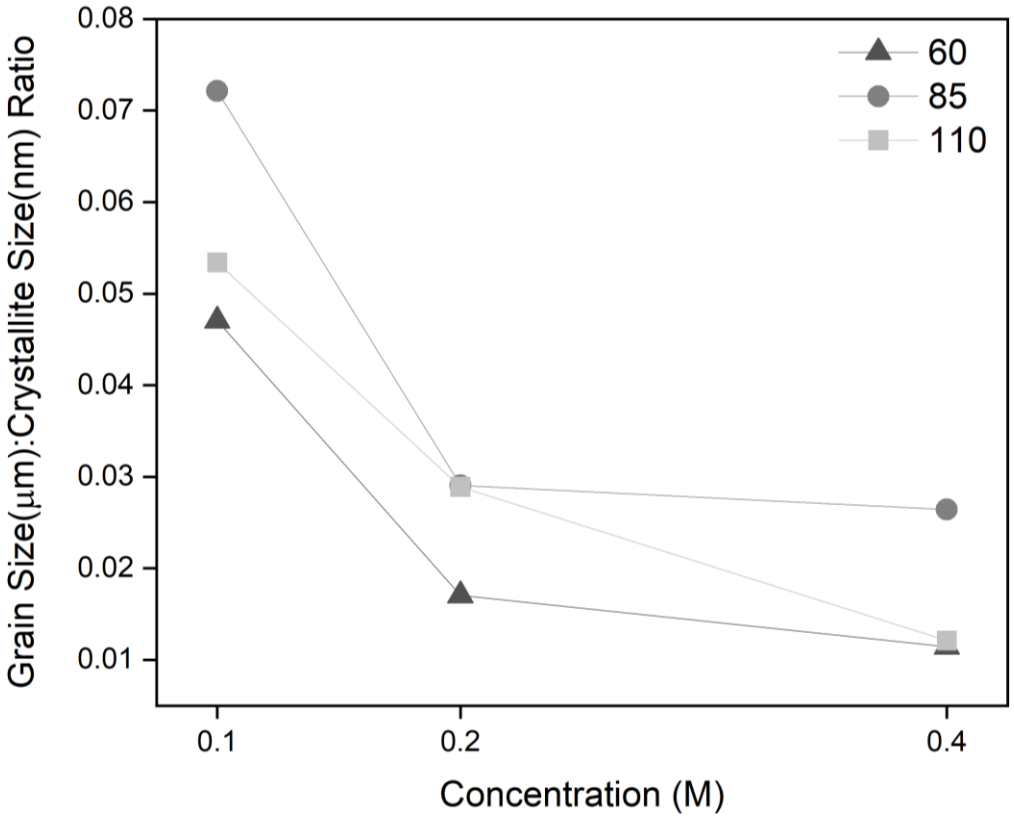

Figure S4: Ratio of grain size (μm) to crystallite size (nm) as a function of mist concentration for the three studied temperatures (60, 85 and 110 ˚C).

Table S2: FWHM, area and reduced chi-squared of the fitted bands in the PL spectra.

Recrystallization Conditions	526 nm Band		541 nm Band		Reduced Chi-Sqrd
	Area	FWHM	Area	FWHM	
As Deposited	0.45252	7.09	0.92875	10.83	1.09×10^{-5}
85 ˚C 0.1 M	0.95422	9.65	0.28	10.03	9.98×10^{-6}

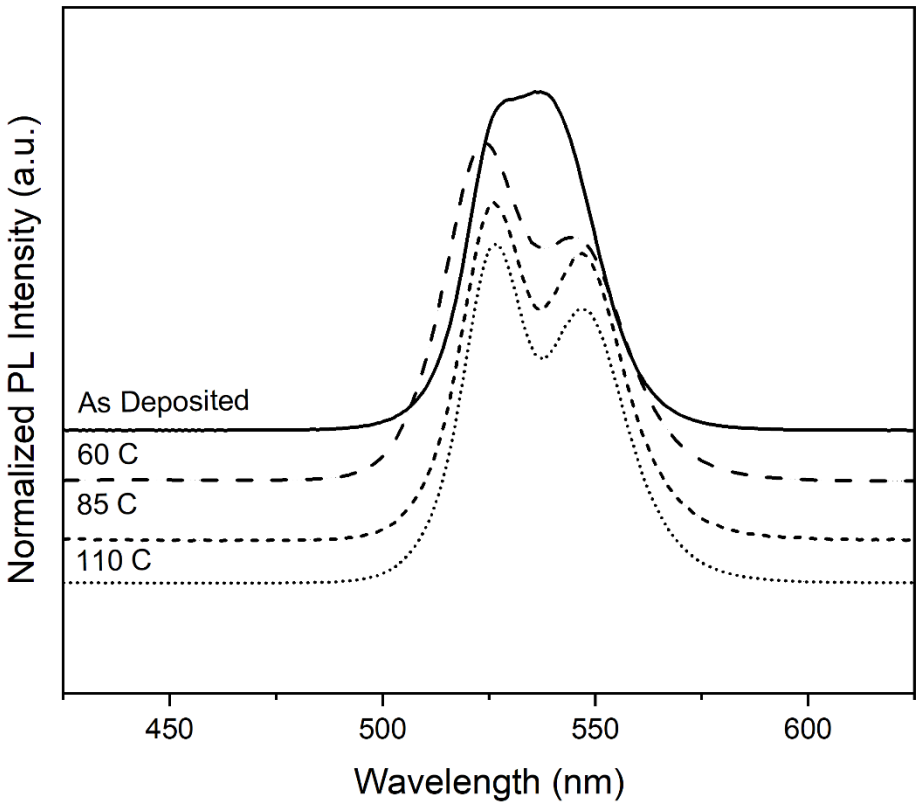

Figure S5: Normalized photoluminescence (PL) spectra of $CsPbBr_3$ films processed via mist-assisted dissolution-recrystallization (MADR). The spectra show the evolution of the optical response as a function of annealing temperature from 60 – 100 °C, at a fixed mist concentration of 0.2 M. The blue shift observed at 60°C correlates with the presence of secondary tetragonal $CsPb_2Br_5$ and rhombohedral Cs_4PbBr_6 phases as identified by XRD (Figure 3 and Figure S2).

Section S2: Sheet Conductance Calculation

The sheet conductance (G_{sheet}) of the device was extracted from the linear current-voltage (I-V) characteristics. The slope of the I-V curve was used to determine the device conductance, and the sheet conductance was calculated using:

$$G_{sheet} = \frac{I}{V} \times \frac{L}{W}$$

where I/V is the slope of the linear I-V curve, L is the channel length, and W is the channel width of the planar Pt/$CsPbBr_3$/Pt device.

Section S3: Responsivity and Detectivity Calculations

The responsivity (R) of the device was calculated from the measured photocurrent and incident optical power using:

$$R = \frac{I_{ph}}{P_{in}}$$

where I_{ph} is the photocurrent, defined as the difference between the illuminated current and the dark current ($I_{illum} - I_{dark}$), and P_{in} is the incident optical power, calculated as the product of the illumination intensity and the device active area ($I \times A$).

The specific detectivity (D*) was calculated assuming shot-noise limited detection:

$$D^* = \frac{R\sqrt{A}}{\sqrt{2qI_{dark}}}$$

where R is the responsivity, A is the active area of the device, q is the elementary electron charge, and I_{dark} is the dark current.

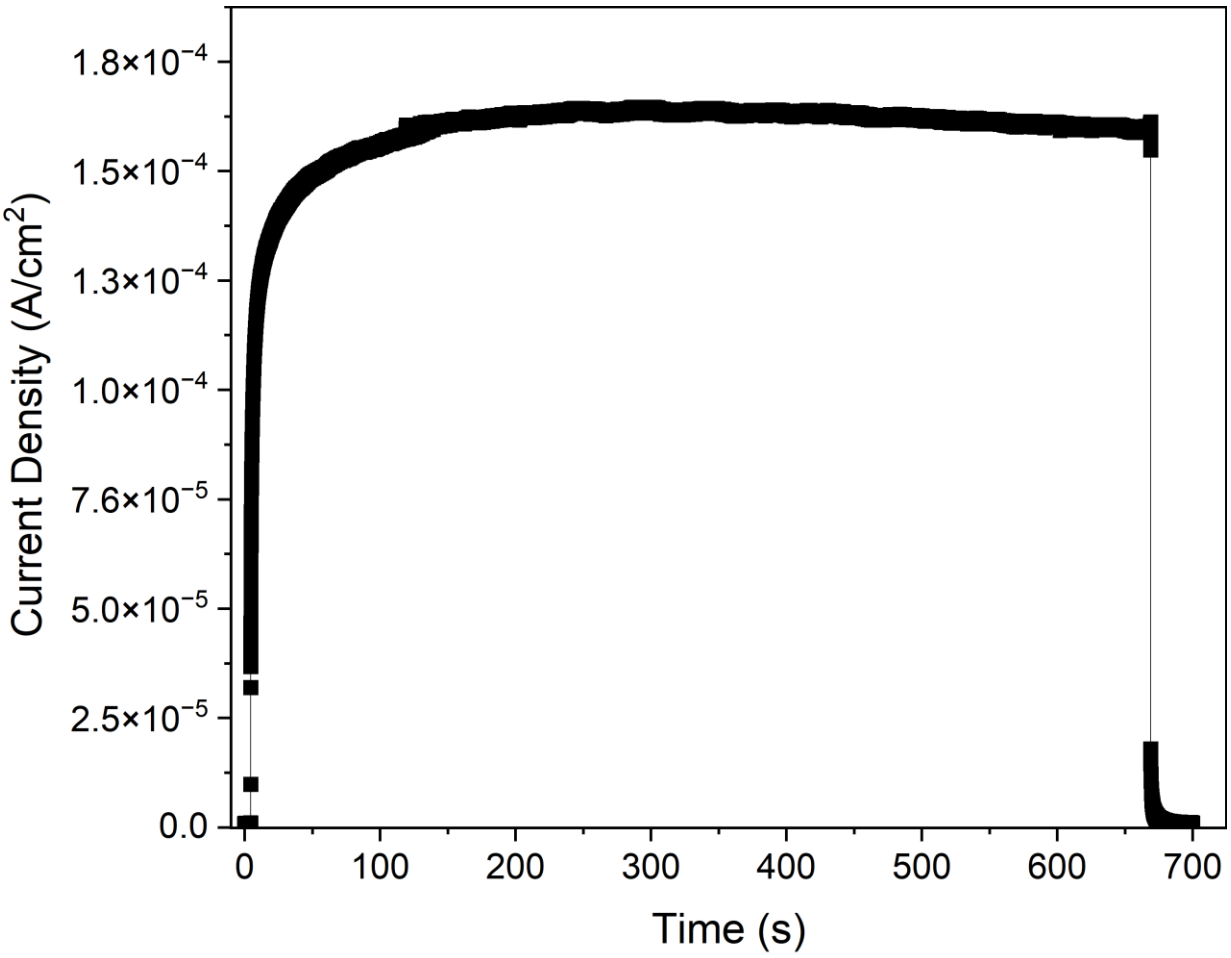

Figure S6: Photocurrent response of the MADR treated film illuminated at 125 mW/cm^2 with a 365 nm LED at -5 V bias voltage, for approximately 10 minutes. This data shows operational stability under extended illumination periods. The photocurrent observed decrease in magnitude of photocurrent response by approximately 100 nA is due to the age of the device (6-month old) after storage in ambient conditions.